Hydrophilic co-assembly of wheat gluten proteins and wheat bran cellulose improving the bioavailability of curcumin

Peng-Ren Zou[1], Fei Hu [1], Fan Zhang [1], Kiran Thakur [1,2], Mohammad Rizwan Khan [3], Rosa Busquets [4], Jian-Guo Zhang [1,2], and Zhao-Jun Wei [1,2]*

[1] School of Food and Biological Engineering, Hefei University of Technology, Hefei 230601, China;

[2] School of Biological Science and Engineering, Collaborative Innovation Center for Food Production and Safety, North Minzu University, Yinchuan 750021, China

[3] Department of Chemistry, College of Science, King Saud University, Riyadh 11451, Saudi Arabia.

[4] School of Life Sciences, Pharmacy and Chemistry, Kingston University London, Kingston Upon Thames KT1 2EE, Surrey, England.

1040744976@qq.com (P.R.Z.);
hufei@hfut.edu.cn (F.H.);
zffs2012@mail.ahnu.edu.cn (F.Z.)
kumarikiran@hfut.edu.cn (K.T.);
mrkhan@KSU.EDU.SA (M.R.K.)
r.busquets@kingston.ac.uk (R.B)
zhangjianguo@hfut.edu.cn (J.G.Z.);
*Correspondence: Zhao-Jun Wei (zjwei@hfut.edu.cn).

ABSTRACT

Low-cost wheat by-products have been modified to become an effective delivery system for curcumin. Wheat bran cellulose (WBC) and wheat gluten proteins (WPs) were co-assembled by a pH cycle and addition of sodium tripolyphosphate (STP). Fluorescence spectroscopy and zeta-potential evidenced that the embedding of WBC into the WPs favored the formation composites a relative unfolding state. Modifying the nanocomposite with STP lowered the Dh and PDI of the co-assembled structure. The nanocomplexes had a typical core–shell structure according to TEM characterization, where proteins aggregate to form a hydrophobic core and the hydrophilic WBC and STP crosslinked to form the shell. To improve the bioavailability of curcumin, it was encapsulated in WWBCs composites by participating in their structural co-assembly. In vitro simulated gastrointestinal digestion experiments showed that the curcumin encapsulated in WWBCs possessed gastrointestinal slow and controlled release function, with a final release of curcumin of 77.8 ± 2.3 %.

Keywords: Wheat gluten proteins; Wheat bran cellulose; pH cycling; Structural assembly; Delivery system

Chemical compounds studied in this article:

Wheat gluten (PubChem SID: 135322122)

1. Introduction

Proteins and polysaccharides have been broadly used as texture modifiers, nutritional supplements or delivery vehicles in the food and cosmetic sectors because of their physico-chemical properties as well as their high biocompatibility and biodegradability. Wheat gluten proteins (WPs) are by-products of processing wheat flour with high-yield and low-cost, and widely used in food processing. WPs are composed mainly of glutenin and gliadin which are rich in essential amino acids and have unique rheological properties when hydrated due to their structure and composition (Yao, Jia, Lu, & Li, 2022). WPs, include in their composition non-polar amino acids (over 35 % of the total amino acids), which tend to form highly polymerized states (due to hydrophobic interactions and disulfide bonds) that result in poor dissolution in water (Wang, Gan, Zhou, Cheng, & Nirasawa, 2017). This leads to unsatisfactory functional properties (e.g., emulsification and gelation) of WPs when in suspension, which severely limits their industrial application in aqueous solution-mediated processing (Ortolan, Urbano, Netto, & Steel, 2022). Therefore, the development of new and effective solubilization techniques for WPs is key to extending their use and increasing their commercial value. Currently, the improvement of aqueous solubility of WPs has been predominantly carried out by modifying the structure of the main and side chains for these proteins by one or more methods. Specifically, these methods involve physical, enzymatic, or chemical modifications that increase the aqueous solubility of WPs. However, they have limitations such as high costs, high nutrient loss and lead to limited gain in solubility (Liao et al., 2010). Therefore, new efficient and green modification technique for increasing the aqueous solubility of WPs is needed.

The molten globule, MG, is an intermediate state between the fully denatured structure and the state where proteins have their natural folding with intact secondary structural units consistent with natural proteins (Wang, Zhang, Wang, Wang, & Chen, 2015). Achieving the relatively unfolded structure of protein in the MG state is important for making key structural modifications to the protein interior. In general, the co-assembly of multiple components to form composites is a viable route for modifying proteins, thereby new properties as well as new structures are achieved (Zhu, Meng, Song, Ding, & Guo, 2022). He, Wang, Feng, Chen, & Wang (2020) found that the WPs was completely soluble in aqueous solutions at pH 12 when co-dissolved with soy protein, and such conditions could promote the MG state of WPs. Compared to enzymatic and chemical modifications, the MG-state transformation of WPs under dilute alkaline environment better to maintain the complete secondary structural units consistent with natural proteins, therefore this method has great potential for the modification of food-grade hydrophobic proteins. However, the induction of MG transformation of WPs by only acid/alkali treatment does not achieve the solubilization of hydrophobic proteins in a single step.

Cellulose has hydrophilic groups that can form intramolecular or intermolecular hydrogen bonds that can play a role in protein-based nanocomplexes (Huang et al., 2016, Jamroz et al., 2014). Indeed, like WPs, wheat bran is another major by-product of wheat processing and it has a high cellulose content of 40–60 % (Zhou et al., 2021). However, a few studies have reported on the development of complexes between the WPs and wheat bran cellulose (WBC) through co-assembly to improve the functional properties of proteins despite the potential of this approach. Furthermore, many studies have found that the polyphosphates (e.g sodium tripolyphosphate) were excellent cross-

linking agents due to their non-toxicity, good biocompatibility, and ability to gel easily, which can induce polysaccharides and their complexes to form stable cross-linked networks (Zhang et al., 2021, Yang et al., 2021). Therefore, polyphosphates can be used as cross-linking agents to enhance the co-assembly of the WPs and WBC into a hydrophilic conformation using pH cycling.

Curcumin is a food nutrient with important health benefits, such as anti-inflammatory, antioxidant and other pharmacological properties. However, due to its hydrophobic structure, curcumin has very low solubility in aqueous solutions (Omidi, Rafiee, & Kakanejadifard, 2021). In addition, curcumin has limited thermal and pH stability, the latter hinders its intestinal absorption. Therefore, it is important to investigate an effective delivery system for curcumin. Co-assembly between wheat gliadin and chitosan could be constructed nanocomplexes that improved the encapsulation efficiency and controlled release of curcumin (Zeng et al., 2019). On this basis, the delivery properties of assembled structures including curcumin with WPs would expand WPs' applications and improve the delivery efficiency of curcumin. The aim of this study was to construct hydrophilic nanocomplexes by pH cycling, according to the principle of co-assembly, between the WPs and WBC to improve the effect on the encapsulation and bioavailability of curcumin.

2. Materials and methods

2.1. Samples and reagents

Wheat gluten was obtained from Wanbang Industrial Company (Zhengzhou, China). Wheat bran was obtained from Ruikang Food Biotechnology Company (Hefei, China). Sodium

tripolyphosphate (STP) was purchased from Maclin Chemical Reagent Co., ltd (Shanghai, China). The rest of chemicals were provided by Sinopharm Chemical Reagent Co., ltd (Shanghai, China) and were of analytical quality. The dialysis bags had 500–1000 MW cut off and were obtained from Nanjing senbejia Biotechnology Co. ltd (Nanjing, China). Water used in this study was deionized.

2.2. Preparation of WPs

Wheat gluten proteins (WPs) were isolated from wheat gluten powder according to a previous method with some modifications (Arte, Huang, Nordlund, & Katina, 2019). Briefly, wheat gluten powder was mixed with water (10 %, w/v). The pH of the dispersion was regulated to 12 with 1 M NaOH and then stirred for 2 h. Next, the solution was centrifuged to remove impurities (7155 rcf for 10 min at 4 °C), such as starch, which remained in the pellet (Centrifuge, HC-3018R, Anhui Zhongke Zhongjia Scientific Instruments Co., Hefei, China). The supernatant was regulated to pH 4.0 with 1 M HCl, and it was centrifuged at 11,180 rcf for 10 min at 4 °C. The precipitate was collected to get the WPs (the content of protein was 87.9 %) and it was freeze-dried. The protein content of WPs sample was determined using the Kjeldahl Nitrogen Determination method.

2.3. Preparation of WBC

Wheat bran cellulose (WBC) was prepared referring the method described by Xiao et al. (2020) with some modifications. Briefly, wheat bran was ground and sieved (0.425 mm). The sieved bran was mixed with water at a ratio of 1:10 (w/v), and the mixture was boiled for 10

min to remove impurities such as phytic acid. The solution was left to cool to room temperature and its pH was regulated to 5.0 with 1 M HCl. Followed, α-amylase at 1.2 % of wheat bran (w/w) was added to that solution for removing starch (60 °C, 2 h). The solution was regulated to pH 11.0 with 1 M NaOH, which inactivated α-amylase. To remove proteins, alkaline protease at 0.6 % of wheat bran was added to the solution (45 °C, 1 h). The solution was finally boiled to inactivate enzymes, cooled down for room temperature and centrifuged (7155 rcf for 10 min at 25 °C). The precipitate, was washed for 3 times sequentially, with 95 % ethanol, 78 % ethanol and acetone (100 %), respectively, then dried to get crude cellulose. After the starch and protein removal, the crude cellulose was added to a 5 % NaOH solution (w/v) at a ratio of 1:20 (w/v) and the mixture was magnetically stirred at 70 °C for 4 h. Then, the mixture was washed with excess water to get the insoluble residue that further was bleached with NaClO2 solution (1.5 %, w/v, pH 3–4) at 75 °C for 5 h with continuous stirring. The pH of mixture was adjusted to pH 3–4 with glacial acetic acid and this maintained the structure of cellulose and obtained cellulose with good water solubility. The resulting white precipitate was washed thoroughly with water to pH 7.0. After washing, the precipitate (WBC) was left to dry on air.

2.4. Preparation of WPs and WBC composites (WWBCs)

WWBCs composites were prepared referring the method of He et al., 2020, Wang et al., 2019. WPs were dispersed in water (2.5 %, w/v) and its pH was regulated to 8.0–9.0 with 2 M NaOH. STP was added to the dispersion at the mass of 2 % (w/v, g/mL). The mixture was left to react at 45 °C for 2 h under magnetic stirring. The pH of the reaction was maintained at 8.0–9.0 by occasional addition of 1 M NaOH. The suspension was dialyzed (500–1000 MW cut off)

with water at 4 °C for 24 h (with no water changes) and then freeze-dried to get phosphorylated WPs.

Phosphorylated WPs and WBC were mixed at a mass ratio of (1:0.1, 1:0.3, 1:0.5, 1:0.7, 1:0.9, w/w) to a final concentration of 5 % (w/v) in every case. The pH of solution was regulated to 8.0–12.0 with 4 M NaOH. Following, its pH was regulated to 7.0 with 1 M HCl in a water bath at 30 ~ 70 °C for 5 ~ 25 min. The neutral solution was centrifuged at 11,180 rcf for 10 min at 4 °C and the supernatant was dialyzed with water for 24 h to get a soluble nanocomplexes solution. The polymer polydispersity index (PDI) and average diameter (Dh) were used during the optimization to explore the preparation conditions of nanocomposite particles. Based on the optimized results, the stable nanocomposite particles were prepared according to the mass ratio of phosphorylated WPs to WBC (1:0.1, 1:0.5 and 1:1), which were named WWBCs0.1, WWBCs0.5 and WWBCs1.0.

2.5. Particle size measurements.

The Dh and PDI of WWBCs composites were determined by Nano-Zetasizer (Nano-ZS90, Malvern ltd, Malvern, UK) at room temperature following a published procedure (Hadidi, Jafarzadeh, & Ibarz, 2021). Nanocomplexes samples were diluted with water to concentrations of 1 mg/mL before the measurements.

2.6. Turbidity determination

Turbidity of 1 mg/mL solutions of WPs, WPs/STP/WBC mixture and chemically

derivatized WPs: WPs-STP, WPs-WBC0.5 (without STP treatment) and WPs-STP-WBC0.5 (obtained according to section 2.4) was determined using a UV–vis spectrophotometer (UV-2600, Shimadzu ltd, Suzhou, China) at 600 nm according (Ru, Wang, Lee, Ding, & Huang, 2012). Measurements were caried out at room temperature (25 °C).

2.7. Structural characterization of WWBCs composites

2.7.1. Fluorescence analysis

The fluorescence spectra of WWBCs were determined by adapting a well-established method (Malavasic, Poklar, Macek, & Vesnaver, 1996). The WWBCs solution was diluted with water to a protein concentration of 0.1 % (w/v). The excitation conditions were 280 nm and the emitted fluorescence spectra was collected between 300 and 400 nm. Thiourea, NaCl and SDS were added to the mixture of WPs and WBC at a final concentration of 10 mmol/L to determine the effects of hydrogen bonding, hydrophobic interactions, and electrostatic interactions in the co-assembled of WPs and WBC.

The exogenous fluorescence of WWBCs was measured using a fluorescence probe (ANS). In the neutralization step of the WWBCs preparation, the solution was taken, diluted to a protein concentration of 0.1 % (w/v) with water. Then the pH of solution was regulated to the corresponding pH with 1 M NaOH. Subsequently, 4 mL of diluted solution containing WWBCs was mixed with ANS (8 mmol/L, 10 μL) solution. In this case spectral data of the emission wavelength were collected from 460 to 560 nm at an excitation wavelength of 390 nm.

184 2.7.2. Surface hydrophobicity

185 The H0 of WWBCs was measured referring the method described by Wang et al. (2016).
186 The solution of each sample was diluted to several concentrations (1, 0.75, 0.5, 0.25 and 0.125
187 times, respectively) with water adjusted to the same pH than the sample. Briefly, 4 mL of diluted
188 solution to be measured was mixed with ANS solution (10 μL, 8 mmol/L). The emission and
189 excitation wavelengths were set to 484 nm and 390 nm, respectively, and the fluorescence
190 intensity of each sample was measured under these conditions. Surface hydrophobicity (H0)
191 was defined as the slope of the fluorescence intensity against protein concentration.

192

193 2.7.3. ζ-potential

194 For the assessment of the changes of the surface potential by ζ-potential, all samples were
195 pre-diluted to 0.1 % (w/v) with water was adjusted to the desired pH. The determination was
196 carried out with Nano-Zeta sizer at 25 °C.

197

198 *2.8. Characterisation of the apparent morphology characteristics of the WWBCs by microscopy*

199 The solution of each sample was diluted onto a copper mesh coated with carbon film
200 followed by the traditional negative staining method. Each sample was observed by
201 transmission electron microscopy (TEM) (JEM1400FLASH, Hitachi, Japan) under the method
202 described by Chen et al., 2021, Chen et al., 2021 at the accelerating voltage of 80 kV.

203 Each sample was fixed to a double-sided tape on a carrier table and then gold-plated onto
204 the surface. The surface morphology of each sample was observed by a Scanning Electron
205 Microscope (SEM) (Regulus 8230, Hitachi, Japan) at an operating voltage of 20

206

207 Each sample solution diluted and added dropwise to a freshly prepared smooth and flat
208 mica sheet, and then it was left to dried at room temperature. The morphology of each sample
209 was further observed using an atomic force microscope (AFM) (Dimension Fastscan, Bruker,
210 Germany) at the scanning frequency of 1 Hz (Wang, Gan, Li, Nirasawa, & Cheng, 2019).

211

212 *2.9. Encapsulation of curcumin in WWBCs*

213 The encapsulation of curcumin in WWBCs composites was prepared referring the method
214 described by Zhang et al. (2022). Curcumin was completely dissolved 4 mg/mL in 0.05 M
215 NaOH. Following, the pH of solution was regulated to 12. The phosphorylated WPs and WBC
216 were mixed at mass ratios of 1:0.1, 1:0.5 and 1:1 to 50 mL total volume and solute concentration
217 of 5 % (w/v). Then, the dissolved curcumin (4 mg/L at pH 12) was added to above mixed
218 solution to final concentration of curcumin of 0.2, 0.5, 1.0 and 2.0 mg/mL in a total volume of
219 100 mL, where the pH of mixture was regulated to 12. Finally, the pH of mixture was slowly
220 regulated to 9 with 0.1 M HCl while stirring immediately in a 60 °C water bath, followed by a
221 further slow (within 10 min) adjustment to pH 7 using 0.02 M HCl. After the mixture was
222 centrifugated at 11,180 rcf for 10 min at 4 °C, the supernatant, which included curcumin
223 encapsulated in WWBCs composites, was collected. The supernatant was filtered to further
224 remove impurities, resulting in the final WWBCs composites. The liquid of WWBCs
225 composites was used directly for encapsulation efficiency, encapsulation capacity, simulated
226 gastrointestinal digestion and DPPH scavenging activity assay determination. A part of
227 WWBCs composites were freeze-dried for X-ray Diffraction、FT-IR and differential scanning

calorimetry analysis.

2.9.1. Stability assessment with UV-Vis and ζ-potential

The degradation of curcumin at pH 12, and the effect of WPs and WBC, WWBCs composites on its degradation rate was monitored with UV–vis. Curcumin was 2 mg/mL that the pH was regulated to 12. Subsequently, 200 μL of curcumin solution was mixed with 40 mL of water (pH 12), WPs, WBC, WWBCs composites (both 1 mg/mL) and the UV spectra of each mixture were measured at regular time intervals between 0 and 60 min.

2.9.2. Determination of WWBCs curcumin encapsulation efficiency (EE) and encapsulation capacity (EC)

The EE and EC were determined referring the method described by Shahgholian & Rajabzadeh (2016) with some modifications. Curcumin was dissolved at 1 mg/mL in anhydrous ethanol solution. This stock solution was diluted further with anhydrous ethanol to make a series of standard solutions (1.0 ~ 10.0 μg/mL). Anhydrous ethanol was used as a blank solution. Standards were measured at 430 nm and they were used to build calibration curve. The EE and EC of curcumin were calculated using the following Eqs (1) and (2).

$$EE(\%, w/w) = \frac{M_{loaded}}{M_{original}} \times 100\% \qquad \text{Equation1}$$

$$EC(mg/g, w/w) = \frac{M_{loaded}}{M_{WWBCs}} \times 100\% \qquad \text{Equation2}$$

where M_{loaded}, $M_{original}$ and M_{WWBCs} represent the amount of encapsulated curcumin, the amount of added curcumin and the mass of WWBCs *composites*, respectively.

250

251 *2.9.3. X-Ray Diffraction (XRD) analysis*

252 The crystalline structure of each sample was characterized with X-ray powder diffraction
253 (model D/MAX 2500 V, Rigaku Corporation, Tokyo, Japan) at 30 kV and 10 mA with Cu-
254 Kα radiation (k = 1.5406 Å). The XRD pattern of each powder sample was scanned from 5°
255 and 60° (2θ) at 2°/min.

256

257 *2.10. FT-IR analysis*

258 The functional groups of the study proteins and complexes were determined with an FT-
259 IR (Nicolet 6700, Thermo Electric Corporation, USA) using 4000-600 cm^{-1} as acquisitions
260 work range. Each sample (1 mg) was mixed with KBr (150 mg) in a mortar. A fraction of the
261 homogenised mixture was scanned at 4 cm^{-1} with 16 scans.

262

263 *2.11. DSC measurements*

264 The thermal properties of each sample were measured by DSC (Q2000, TA instruments,
265 USA) referring the method described by Chen et al. (2021). Each sample of approximate 5 mg
266 was weighed into a crucible, and the empty crucible was used as a control. All sample were
267 heated at 10 °C/min from 30 °C to 200 °C with nitrogen flowing at 50 mL/min and the test
268 carried out in triplicate.

269

270 *2.12. Simulated gastrointestinal digestion*

271 The kinetics of curcumin release from WWBCs composites was investigated by simulated

gastrointestinal conditions, including simulated intestinal fluids (SIF, pH 7.4) and gastric (SGF, pH 2) according to the method described by Hu et al. (2021). The SGF or SIF was mixed with equal volume of ethanol as a release medium. Curcumin powder dispersion or freshly prepared nanocomplexes (CUR-WWBCs) and simulated SGF release medium were pre-warmed for 10 min at 37 °C. The curcumin powder dispersion or CUR-WWBCs was placed in dialysis bags (10 kDa molecular cut off), and then immersed in 100 mL of simulated SGF release medium under magnetic stirring. After the mixture was incubated in an oscillator at 37 °C for 2 h, the dialysis bags were placed in 100 mL of simulated SIF release medium and then incubated in an oscillator at 37 °C for 4 h. Throughout the incubation period, 1 mL of release medium every 15 min was collected to determine curcumin concentrations. At the same time, an equal amount of fresh medium was supplemented to replace the sample taken and keep constant volume of release medium.

2.13. DPPH (2,2-diphenyl-1-picrylhydrazyl) scavenging activity assay

The DPPH radical scavenging activity of CUR-WWBCs was measured as described earlier (Liu, Li, Yang, Xiong, & Sun, 2017) with some modifications. The DPPH reagent was prepared in anhydrous ethanol to a final concentration of 100 μM. DPPH ethanol solution (4 mL, 100 μM) was mixed with equal volume of curcumin aqueous solution, curcumin ethanol solution and CUR-WWBCs solution, respectively. The reaction of each mixture was carried out for 30 min at room temperature and protected from light. The absorbance of each solution was measured at 517 nm. The free radical scavenging rate of each sample was calculated according to Equation 3:

$$DPPH\ Scavenging\ (\%) = 1 - \frac{A_t - A_b}{A_c}$$ Equation 3

Where, A_t is absorbance of samples at different times (CUR-WWBCs solution and DPPH solution mixed in equal volumes); A_b is absorbance of the sample (CUR-WWBCs solution and ethanol solution mixed in equal volumes); A_c is absorbance of sample (water and DPPH solution mixed in equal volumes)

2.14. Statistical analysis

All the experiments were conducted in triplicates and results are given as mean ± standard deviation. The experimental data were processed and analyzed by SPSS software, and statistical analysis was executed using one-way analysis of variance with a significance level of 0.05 and graphs were plotted using Origin 2018 software.

3. Results and discussion

The challenge of preparing efficient and stable delivery systems for curcumin using nanocomplexes that included by-products from wheat production (WPs, WBC) has required investigating main factors influencing the interaction between the WPs and WBC using complementary techniques. The performance of the novel nanocomplexes as curcumin delivery system has been evaluated

3.1. Preparation of WWBCs composites

WPs, both dissociated and co-assembled with WBC, were induced to form dispersible nanocomplexes by pH cycling induction. Fig. 1A displays the effect of pH on particle size (Dh) of the formed nanocomplexes and polymer dispersion index (PDI). Both parameters decreased as the pH of the mixed solution approached 12 and then it was neutralized. Such critical pH

induced sufficient dissociation of protein subunits, subsequently favoring WP co-assembling with WBC into smaller and stable nanocomplexes induced by the neutralization step. Hence pH 12 was taken as optimal pH to induce the formation of nanocomplexes. In contrast, less basic pH conditions did not cause sufficient dissociation of WP subunits and WP co-assembled with WBC into larger and unstable nanocomplexes due to their strong hydrophobic attraction.

The isoelectric point of WPs is pH 6.0-8.0. The number of cations in these proteins increased as the pH of the solution was acidified. As the pH of mixed solution got closer to neutrality (from pH 12 to 7), the positively charged regions of WPs combined with anionic in WBC, which led to assembling into nanocomplexes. The Dh of nanocomplexes raised with the increase of the concentration of WBC (Fig 1B). However, the PDI of nanocomplexes was not linear with the concentration of WBC: at greater concentration of WBC, WPs combined more with WBC, thus increasing the Dh of the nanocomplexes formed between both biomolecules. As the pH of mixed solution was neutralized, WP aggregated to form macroscopic flocs. However the presence of WBC inhibited the formation of such flocs, resulting in well-stabilized nanocomplexes. Considering the variation of Dh and PDI, the ratio of WP to WBC was adjusted to 1:0.5 for the optimal preparation of nanocomplexes constituted by WP and WBC.

To enhance the interaction between WP and WBC in the system, the effect of heating in a water bath during the pH cycling was tested (Fig. 1C). Dh and PDI of the nanocomplexes formed did correlate with increasing temperature for most of the temperature ranged studied. At 60°C, PDI reached minimum values, hence such conditions favoured the preparation of stable nanocomplexes with uniform particle size distribution. The Dh of the nanocomplexes gradually increased with the duration of the neutralization step from 12 to 7 (shown in Fig. 1D,

t). However, the opposed effects of nanocomplexes' PDI before gradually stabilizing. This indicated that WP co-assembled with WBC to form more stable nanocomplexes with increasing time, resulting in nanocomplexes with a narrow distribution of particle size. Therefore, a conditioning time of 10 minutes was chosen to ensure that the resulting nanocomplexes were more homogeneous in size and stable.

The effect of STP modification on the Dh and PDI of nanocomplexes was shown in Fig. 1E. The Dh of modified WP by STP modification was greater than that of original WP. This may be because STP could interact with WP resulting in increasing the exposure of more amino acid residues and favoring the formation of covalent bonds. Importantly, the Dh of nanocomplexes after STP modification co-assembled with WPs and WBC was smaller than that of nanocomplexes without STP modification. This suggested that the STP crosslinked with WP or WBC to form a triple network structure, resulting in tighter interactions within nanocomplexes and particle shrinkage, which in turn lead to a reduction in particle size. In addition, the PDI of nanocomplexes with STP modification was lower than that of nanocomplexes without STP modification, indicating that STP modification of WP can improve the level of dispersibility for nanocomplexes. As the pH of solution approached 7, WP tended to aggregate to form macroscopic soluble precipitates under hydrophobic action, resulting in lower light transmission and higher turbidity. As can be seen in Fig. 1F, the WP/STP/WBC mixture behaved similarly to WP, indicating that STP and WBC were unable to prevent WP aggregation in the absence of covalent interaction. However, light transmission of nanocomplexes with STP modification was significantly higher than that without STP modification, suggesting that STP can not only bind to WP to form complex, but also cross-link

with WBC to form soluble nanocomplexes.

3.2. Structural characterization of WWBCs composites

3.2.1. Fluorescence spectra

The binding of proteins to exogenous substances such as polysaccharides can induce electron transfer from the electron-rich aromatic amino acids to the electron-deficient amino acid chromophores, resulting in fluorescence quenching. Thus, fluorescence quenching of protein can be used to evidence whether it is binding with another substance. In order to distinguish the pH cycle-induced structural co-assembly from a simple mixture of two substances, interaction between WP and WBC was tested using endogenous fluorescence spectroscopy. The fluorescence intensity of WWBCs composites was completely derived from WP due to WBC not having luminescent groups. As shown in Fig. 2A, the fluorescence intensity of WWBCs composites was lower than that of WP. Furthermore, the extent of quenching was related to the increase of WBC concentration, indicating that WBC was not involved in the structural self-assembly of WP via a pH cycle. Compared to a single WP, the fluorescence spectrum of WWBCs was red-shifted, suggesting that the formation of this co-assembly structure led to a decrease in the hydrophobicity of microenvironments with groups such as tryptophan and tyrosine, which increased the stability of the complexes. Thus, co-assembled structure of WWBCs can increase the solubility of WP facilitating it stability in aqueous solution. To determine the main forces driving the formation of WWBCs composites, thiourea, SDS and NaCl were added to block hydrogen bonds, hydrophobic interactions and electrostatic interactions, respectively. As shown in Fig. 2B, the fluorescence intensity of mixed solution after the addition of blockers was stronger than that of WWBCs without salts,

382 indicating that ionic interactions drive the co-assembly between WP and WBC. Among them,
383 the highest fluorescence intensity was observed for WWBCs with SDS addition, indicating that,
384 besides electrostatic interactions, hydrophobic interactions were also an important contributor
385 to this co-assembly behavior.

386 The fluorescent probe bound to the hydrophobic region of protein through hydrophobic
387 interactions in response to changes in the protein microstructure and polarity of surrounding
388 environment. WP was induced to transform into a MG state by dilute alkali at pH 12, and the
389 change in ANS fluorescence intensity during its neutralization was shown in Fig. 2C. The peak
390 fluorescence emission of WWBCs composites was at 474 nm for pH 12 , conditions where the
391 structure of WP was relatively unfolded. Such conditions facilitated ANS binding the
392 hydrophobic region of the complexes. As the pH decreased, the ANS affinity was expected to
393 decline because the hydrophobic region would encapsulate as the protein refolded. However,
394 the fluorescence intensity of WWBCs composites increased as the neutralization reaction
395 proceed. This might be attributed to WP exposing hydrophobic regions and the conformation
396 of WWBCs composites remaining relatively unfolded, which allows the ANS probe to enter
397 the conformation and bind to the hydrophobic regions.

398 The polarity of microenvironment within WWBCs changed with pH, and this was
399 observed by a reduction in the wavelength of the maximum fluorescence emission when
400 decreasing pH. The ANS fluorescence intensity of the WWBCs composites was significantly
401 lower than that of single WP (Figure 2D). With the increase of the WBC concentration, the
402 fluorescence intensity also continuously decreased and the wavelength of the fluorescence
403 emission increased, indicating that the WBC inhibited the formation of hydrophobic region,

404 thereby contributing to the self-assembly of WP into a hydrophilic conformation. Hence, the
405 WP combined with WBC to construct hydrophilic three-dimensional conformation with the pH
406 cycle.

407 *3.2.2. Surface properties of WWBCs composites*

408 Protein folding tended to expose charged groups while encapsulating hydrophobic groups
409 internally. In order to further explore formation mechanism of WWBCs composites, the surface
410 hydrophobicity and zeta-potential of WWBCs were characterized to clarify the structural
411 changes of WPs during co-assembly. With the decrease of pH, the surface hydrophobicity of
412 WWBCs composites increased and the zeta-potential was less negative (shown in Fig. 2E and
413 Fig. 2G). This supports those proteins aggregated at pH 7 due to high hydrophobicity and low
414 zeta-potential. With the increase of WBC concentration, the surface hydrophobicity of WWBCs
415 decreased and the zeta-potential increased, indicating that the structure of WPs remained
416 relative unfolded after assembly with WBC and this prevented the formation of hydrophobic
417 regions and exposed the charged groups inside molecule (Fig. 2F and Fig. 2H). This may have
418 been caused by covalent bonding of hydrophilic phosphate groups and polysaccharide
419 fragments to proteins, which separated hydrophobic regions. In addition, the charge on the
420 surface of WWBCs generated inter-particle electrostatic repulsion, and this could inhibit the
421 tendency of nanocomplexes to aggregate and maintain their stable dispersion in water. It can
422 be concluded that the WBC embedded in WWBCs composites supported the co-assembly
423 structure through electrostatic repulsion, enhancing the rigidity of WPs side chains and thus
424 inhibiting folding.

425 *3.3. Morphological characteristics of WWBCs composites*

426 *3.3.1. TEM*

427 The morphology of WWBCs composites was examined by TEM to clarify microstructural
428 changes of WPs before and after co-assembly with WBC. Compared to WPs, WWBCs
429 composites exhibited core–shell structure (see Fig. 3A-D). The internal lining of WWBCs
430 composites was high and relatively homogeneous, while a relatively loose ring-like structure
431 could be clearly observed at the external edges, indicating that the co-assembly of WPs and
432 WBC formed spherical nanocomplexes with a relatively dense core and a relatively loose shell.
433 This indicates that, the outer WPs hydrophilic groups were hydrophobically crosslinked under
434 potential resistance and the internal hydrophobic amino acids formed the core structure under
435 the preparation conditions. In addition, the hydrophilic polysaccharide fragments and
436 hydrophilic phosphate groups bound to WPs formed the shell structure on the core surface. This
437 is in agreement with recent findings where soy protein modified with succinic anhydride
438 combined with dextran formed nanogel with core–shell structure by the thermal induction
439 method, where the hydrophobic soy proteins where at the core (formed by crosslink) and the
440 hydrophilic dextran chains formed the shell on the core surface (He et al., 2022).

441 *3.3.3. AFM*

442 The micromorphology of WWBCs composites was further observed by AFM. As shown
443 in Fig. 3a~d, WP presented surface morphological characteristics of proteins, indicating that
444 the single WP, without co-assembly with WBC, aggregated into spherical structures after pH
445 cycling treatment. With the addition of WBC, WP co-assembled with WBC to form irregularly
446 shaped nanocomplexes, hence WBC became adsorbed onto the surface of proteins, thereby
447 changing their shape. Furthermore, compared to the WP, the aggregation of WWBCs can also

increased, indicating that there was some interaction between WP and WBC to bind together. When the mass ratio of WP to WBC was 1:0.5, the microstructure of WWBCs showed a more regular oval shape with uniform dispersion. Therefore, at this ratio, WBC interacted well with WP to form stable nanocomplexes.

3.3.2. SEM

The morphology of WP, WBC and WWBCs composites was observed by SEM. The WP showed a smooth surface structure (shown in Figure 4) while the WBC exhibited the rougher and striped surface structure. After the co-assembly of WP and WBC was induced by pH cycling, the microstructure of WWBCs composites mainly showed a spherical structure with chain-like structure embedded on the surface. This points out that WP crosslinked with WBC to form a network where hydrophilic polysaccharide fragments of WBC became embedded in WP to form the shell. The microstructure of WWBCs composites remain similar as the mass ratio of WBC increased. However, at a mass ratio of WP:WBC = 1:0.5, the surface of WWBCs composites showed a regularly arranged chain-like structure, which is indicative that WP and WBC were fully crosslinked to form a tight network structure through interaction at this ratio.

3.4. Characterization of curcumin-encapsulated WWBCs composites

3.4.1. Effect of WWBCs encapsulation on the structure of curcumin

Curcumin is less stable and prone to degradation in alkaline environments. Ultraviolet (UV) spectroscopy was used to measure the effects of dilute alkaline treatment; pH 12, WP, WBC and inter-component reactions on its stability. The UV absorption changes of curcumin solution at pH 12 from 0 to 1h are shown in Fig. 5A. The maximum absorption of curcumin

appeared at 470 nm and its peak intensity decreased continuously with time, which was consistent previous results (Pan, Luo, Gan, Baek, & Zhong , 2014). The UV peak intensity of single curcumin solution decreased by 20.6% after 1h. The degradation rate was 2.0 % when curcumin was mixed with WP solution (Fig. 5B). This suggests that the protein conformation unfolded in dilute alkaline environment had a protective effect on curcumin. In addition, as shown in Fig. 5C and Fig. 5D, the degradation rate of curcumin mixed with WWBCs solution decreased to 5.1% compared to the degradation of curcumin mixed with WBC solution (6.9%). Therefore, the co-assembly nanocomplexes formed by the WP and WBC was able to maintain the stability of curcumin in alkaline aqueous solutions compared to curcumin solution.

3.4.2. EE and EC

Different nanotechnology-based delivery systems, such as nanoliposomes, nanoparticles, and nanohydrogels have been used to encapsulate curcumin and to try improve its poor water solubility and low bioavailability, which was achieved up to a maximum EE of 90 % (Vijayan, Shah, Muley, & Singhal, 2021). Curcumin, like WPs, was soluble in dilute alkaline solutions despite that it was insoluble in water. Therefore, curcumin could participate in the structural co-assembly of WPs and WBC, and the encapsulation of curcumin could be accomplished simultaneously during the structural construction of WWBCs composites. As shown in Fig. 6A and Fig. 6B, when curcumin was added at 0.2, 0.5, 1.0 and 2.0 mg/mL, the EE of WWBCs composites ranged from 42.4 % to 68.7 % and the EC from 17.0 to 59.3 mg/g. The EE decreased with the increase of curcumin concentrations at constant mass ratios of WPs to WBC. However, when the mass ratio of WPs to WBC was 1:0.5, the EE was up to 55.9 % when the concentration of curcumin increased to 2.0 mg/mL, demonstrating the effective encapsulation of curcumin by

WWBCs composites. Under the condition of constant curcumin concentration, the EE of WWBC improved with the increase of WBC concentration in solution. The more WBC there is in solution, the more sites WWBCs has that interact with curcumin during the co-assembly of WPs and WBC induced by pH cycling. The EC increased with the increase of curcumin concentration (shown in Fig. 6-B). Furthermore, at constant curcumin concentration, the EC improved with the increase of WBC concentration. This is because the core of nanocomplexes in the core–shell structure formed by the co-assembly of WPs and WBC had more hydrophobic space, thus facilitating the encapsulation of more curcumin. These results evidence that WPs was able to co-assemble with WBC to achieve effective encapsulation of curcumin-like hydrophobic active substances through pH cycling-induced coiling and folding.

3.4.3. XRD

The XRD patterns of curcumin, WWBCs, and WWBCs encapsulated with curcumin were separately measured to determine the encapsulation effect. The crystalline structure of natural curcumin presented multiple characteristic diffraction peaks between $2\theta = 8.9°$ and 29.1° (Fig. 6C), hence curcumin was in ordered state. WWBCs encapsulated with curcumin presented the same pattern as WWBCs (without curcumin): there was absence of the characteristic peaks belonging to curcumin. This could indicate that the pH cycle-induced encapsulation of curcumin made the transformation of its ordered crystalline structure into an amorphous state, and curcumin was completely encapsulated into the cross-linked structure of WWBCs or that the sensitivity of the analysis was limited to detect curcumin embedded in the complex. These results are in agreement with recent findings where curcumin entrapped in the hydrophobic

514 reservoir of rice proteins could not be detected (Xu, Qian, Wang, Chen, & Wang, 2022).

515

516 *3.5. FTIR*

517 FTIR supported the elucidation of mechanisms of nanocomplexes formation and
518 encapsulation of curcumin. The bands between 3100-3450 cm^{-1} were attributed to the stretching
519 vibrations of -OH, $-NH_2$ and $-CONH_2$. The WWBCs composite, with and without curcumin-
520 embedded, had stronger characteristic signals in that region compared to the WP, and the signals
521 were shifted as a result to different bond environment resulting from chemical derivatisation
522 (Fig. 6D). The presence of these characteristic groups resulted in strong inter- and intra-
523 molecular hydrogen bonding interactions of the WWBCs nanocomplexes. In addition, the
524 absorption peak of -OH at 3407 cm^{-1} became wider and more intense in the WWBCs composite
525 embedding curcumin, possibly from the phenols in curcumin. The region between 1400-1700
526 cm^{-1} included characteristic peaks of the amide I and amide II regions, hence amide bonds
527 formed. Compared to the WP, WBC, and curcumin, there were some differences in the
528 characteristic peaks of amide bonds for the WWBCs composites with and without embedded
529 curcumin, possibly due to electrostatic interactions between WP, WBC, and curcumin. This was
530 consistent with the results for zeta potential, which indicated that the surface potential
531 significantly changed with the addition of WBC. Furthermore, the WWBCs composites of
532 curcumin-embedded lacked the characteristic bands of curcumin, indicating that curcumin was
533 encapsulated in the nanocomplexes, or that its concentration in the embedded form was below
534 the sensitivity limit of FTIR.

535

3.6. DSC

The thermal stability of WWBCs and those with encapsulated curcumin were investigated by DSC. The thermal denaturation temperature (Tp) and molar enthalpy (ΔH) of WWBCs raised with the increase of WBC concentration compared to the WP (included in Table 1). The increase of Tp for WWBCs indicates a gain of thermal stability. In addition, greater ΔH indicas that greater energy is required to break their structure. Furthermore, WBC can form a tight structure with the carbonyl group of proteins through covalent bonding due to the side chain of WBC having a number of hydroxyl groups, which is related to the composite improved thermal stability. This result agree with a previous study where polysaccharides improved the thermal stability of proteins by co-assembly (Zheng et al., 2022) t). Compared to the WWBCs composites, the WWBCs composites with encapsulated curcumin had higher Tp and ΔH: the encapsulation of curcumin formed packed and stable structure. This may be because the complex formation of curcumin with WWBCs through hydrophobic interaction enhanced the hydrophobic interaction and the degree of aggregation within the WWBCs molecules, thus increasing the force of WWBCs molecules to maintain their tertiary structure.

3.7. The release of curcumin in a simulated gastrointestinal environment

The release of WWBCs nanocomplexes including curcumin in simulated gastrointestinal tract medium are shown in Fig. 6E. From the release profile, in the first 2 h of SGF, pure curcumin had a quick release profile (reaching 83.9 ± 2.4 %) and continued to be released quickly upon entering SIF that was completely released within 1 h. However, the release rate of curcumin from its encapsulated form in the WWBCs nanocomplexes in SGF was relatively low, reaching

21.8 ± 1.4 % after 2 h. The release of curcumin takes place by the action of pepsin in SGF. Pepsin cleaves peptide bonds in proteins and the degraded proteins can aggregate and precipitate, resulting in the release of curcumin. Therefore, the core–shell structure of WWBCs nanocomplexes protected the hydrophobic amino acids in the system, delaying and preventing their destruction by pepsin. In addition, the spatial site-block generated by the hydrophobic core of WPs and the hydrophilic shell of WBC in the nanocomplexes may prevent pepsin from digesting curcumin and this leads to the release of limited amounts of curcumin. In the SIF environment, the release rate of curcumin increased, with a quickly release in the early stages and a sustained slow release in the later stages, resulting in a final release rate of 77.8 ± 2.3 %. This may be due to that the co-assembly structure of WWBCs nanocomplexes unfolded, causing a weakened hydrophobic interaction between WPs and curcumin, leading to curcumin release. The later release of curcumin remained invariable, suggesting that the WPs and unreleased curcumin were tightly bound through hydrophobic interactions. These results suggested that the core–shell structure of WWBCs can releasing curcumin under intestinal pH conditions by protecting it from gastric pH degradation, thus effectively enhancing the efficiency and bioavailability of curcumin targeting to the intestine.

3.8 Antioxidant activity of curcumin loaded composites

At the same curcumin concentration, the free radical scavenging capacity of curcumin that was encapsulated in WWBCs nanocomplexes was much greater than that of free curcumin in water (Fig. 6F). In addition, the free radical scavenging capacity of curcumin that was encapsulated in WWBCs nanocomplexes at a mass ratio of 1:0.5 between the WPs and WBC was

approximately equal to that of curcumin-ethanol solution. Compared to the other two ratios, 1:0.1 and 1:1.0, the WWBCs nanocomplexes exhibited greater free radical scavenging at 1:05. Free curcumin was almost insoluble in water: it forms crystals and its antioxidant capacity drops. In contrast, encapsulated curcumin nanocomplexes had increased solubility in water, thus increasing its antioxidant capacity. This indicated that the encapsulation technique via nanocomplexes significantly improved the original poor water solubility of curcumin and exposed more phenolic hydroxyl groups in curcumin, which can trap free radicals. In addition, WWBCs nanocomplexes also had some antioxidant capacity due to their unsaturated double bonds.

4. Conclusion

WPs and WBC were co-assembled to form WWBCs by pH cycling treatment. WBC participated as a filler in the assembly process of WPs and provided electrostatic repulsion that inhibited protein folding. WWBCs presented a core–shell structure, where proteins aggregated to form a hydrophobic core and hydrophilic WBC and STP crosslinked to form the shell. Curcumin was introduced as part the structural co-assembly of WPs and WBC during the formation of the WWBCs composites. The WWBCs composites with encapsulated curcumin had higher thermal stability than in absence of curcumin. The EE of WWBCs nanocomplexes was 55.9 % when the mass ratio of WPs to WBC was 1:0.5 and the starting concentration of curcumin was 2 mg/mL, which improves the problem of low water solubility for curcumin. In vitro simulated gastrointestinal digestion experiments led to a released of only 21.8 ± 1.4 % of curcumin from the nanocomplexes in the stomach, with a final release rate of nearly 80 % of

curcumin after a slow sustained release. The core–shell structure of WWBCs plays a key role in the slow release of curcumin (by slowing the action of pepsin) and protecting curcumin from the pH of the media. This study finds a solution to the problem of WPs use in aqueous solution, gives a new perspective on the mechanisms of protein-polysaccharide interactions, and proposes an effective nanocomplexes for the encapsulation and release of curcumin that can improve its bioavailability.

Acknowledgement

This study was supported by the Key Research and Development Projects of Anhui Province (202104f06020026, 202004a06020042, 202004a06020052, 201904a06020008), the Researchers Supporting Project King Saud University (Riyadh, Saudi Arabia) (RSP-2021/138).

Conflict of interest: None to declare

References

Arte, E., Huang, X., Nordlund, E., & Katina, K. (2019). Biochemical characterization and technofunctional properties of bioprocessed wheat bran protein isolates. *Food Chemistry, 289*, 103-111. https://doi.org/10.1016/j.foodchem.2019.03.020

Chen, S., Ma, Y. C., Dai, L., Liao, W. Y., Zhang, L., Liu, J. F., & Gao, Y. X. (2021). Fabrication, characterization, stability and re-dispersibility of curcumin-loaded gliadin-rhamnolipid composite nanoparticles using pH-driven method. *Food Hydrocolloids, 118*, 1-11. https://doi.org/10.1016/j.foodhyd.2021.106758

Chen, S. X., Ni, Z. J., Thakur, K., Wang, S. Y., Zhang, J. G., Shang, Y. F., & Wei, Z. J. (2021). Effect of grape seed power on the structural and physicochemical properties of wheat gluten in noodle preparation system. *Food Chemistry, 355*, 1-10. https://doi.org/10.1016/j.foodchem.2021.129500

He, J., Chen, Z. X., Gu, Y., Li, Y. N., Wang, R., Gao, Y., Feng, W., & Wang, T. (2020). Hydrophilic co-assemblies of two hydrophobic biomolecules improving the bioavailability of silybin. *Food & Function, 11*(12), 10828-10838. https://doi.org/10.1039/D0FO01882A

He, J., Wang, R., Feng, W., Chen, Z. X., & Wang, T. (2020). Design of novel edible hydrocolloids by structural interplays between wheat gluten proteins and soy protein isolates. *Food Hydrocolloids, 100*, 1-9. https://doi.org/10.1016/j.foodhyd.2019.105395

He, M., Teng, F., Chen, H., Wu, C., Huang, Y., & Li, Y. (2022). Fabrication of soy protein isolate-succinic anhydride-dextran nanogels: Properties, performance, and controlled release of curcumin. *Lwt, 160*, 1-10. https://doi.org/10.1016/j.lwt.2022.113259

Hu, G., Batool, Z., Cai, Z. X., Liu, Y. Y., Ma, M. H., Sheng, L., & Jin, Y. G. (2021). Production of self-assembling acylated ovalbumin nanogels as stable delivery vehicles for curcumin. *Food Chemistry, 355*, 1-8. https://doi.org/10.1016/j.foodchem.2021.129635

Huang, X. X., Huang, X. L., Gong, Y. S., Xiao, H., McClements, D. J., & Hu, K. (2016). Enhancement of curcumin water dispersibility and antioxidant activity using core-shell protein-polysaccharide nanoparticles. *Food Research International, 87*, 1-9. https://doi.org/10.1016/j.foodres.2016.06.009

Jamroz, E., Para, G., Jachimska, B., Szczepanowicz, K., Warszynski, P., & Para, A. (2014). Albumin-furcellaran

complexes as cores for nanoencapsulation. *Colloids and Surfaces a-Physicochemical and Engineering Aspects, 441*, 880-884. https://doi.org/10.1016/j.colsurfa.2013.01.002

Liao, L., Liu, T. X., Zhao, M. M., Cui, C., Yuan, B. E., Tang, S., & Yang, F. (2010). Functional, nutritional and conformational changes from deamidation of wheat gluten with succinic acid and citric acid. *Food Chemistry, 123*(1), 123-130. https://doi.org/10.1016/j.foodchem.2010.04.017

Liu, C. Z., Li, M., Yang, J., Xiong, L., & Sun, Q. J. (2017). Fabrication and characterization of biocompatible hybrid nanoparticles from spontaneous co-assembly of casein/gliadin and proanthocyanidin. *Food Hydrocolloids, 73*, 74-89. https://doi.org/10.1016/j.foodhyd.2017.06.036

Malavasic, M., Poklar, N., Macek, P., & Vesnaver, G. (1996). Fluorescence studies of the effect of pH, guanidine hydrochloride and urea on equinatoxin II conformation. *Biochimica et biophysica acta, 1280*(1), 65-72. https://doi.org/10.1016/0005-2736 (95) 00278-2

Ortolan, F., Urbano, K., Netto, F. M., & Steel, C. J. (2022). Chemical and structural characteristics of proteins of non-vital and vital wheat glutens. *Food Hydrocolloids, 125*, 1-10. https://doi.org/10.1016/j.foodhyd.2021.107383

Pan, K., Luo, Y. C., Gan, Y. D., Baek, S. J., & Zhong, Q. X. (2014). pH-driven encapsulation of curcumin in self-assembled casein nanoparticles for enhanced dispersibility and bioactivity. *Soft Matter, 10*(35), 6820-6830. https://doi.org/10.1039/C4SM00239C

Ru, Q. M., Wang, Y. W., Lee, J., Ding, Y. T., & Huang, Q. R. (2012). Turbidity and rheological properties of bovine serum albumin/pectin coacervates: Effect of salt concentration and initial protein/polysaccharide ratio. *Carbohydrate Polymers, 88*(3), 838-846. https://doi.org/10.1016/j.carbpol.2012.01.019

Shahgholian, N., & Rajabzadeh, G. (2016). Fabrication and characterization of curcumin-loaded albumin/gum arabic coacervate. *Food Hydrocolloids, 59*, 17-25. https://doi.org/10.1016/j.foodhyd.2015.11.031

Wang, K. Q., Luo, S. Z., Cai, J., Sun, Q. Q., Zhao, Y. Y., Zhong, X. Y., Jiang, S. T., & Zheng, Z. (2016). Effects of partial hydrolysis and subsequent cross-linking on wheat gluten physicochemical properties and structure. *Food Chemistry, 197*, 168-174. https://doi.org/10.1016/j.foodchem.2015.10.123

Wang, T., Zhang, H., Wang, L., Wang, R., & Chen, Z. X. (2015). Mechanistic insights into solubilization of rice protein isolates by freeze-milling combined with alkali pretreatment. *Food Chemistry, 178*, 82-88. https://doi.org/10.1016/j.foodchem.2015.01.057

Wang, Y. Q., Gan, J., Li, Y., Nirasawa, S., & Cheng, Y. Q. (2019). Conformation and emulsifying properties of deamidated wheat gluten-maltodextrin/citrus pectin conjugates and their abilities to stabilize beta-carotene emulsions. *Food Hydrocolloids, 87*, 129-141. https://doi.org/10.1016/j.foodhyd.2018.07.050

Wang, Y. Q., Gan, J., Zhou, Y., Cheng, Y. Q., & Nirasawa, S. (2017). Improving solubility and emulsifying property of wheat gluten by deamidation with four different acids: Effect of replacement of folded conformation by extended structure. *Food Hydrocolloids, 72*, 105-114. https://doi.org/10.1016/j.foodhyd.2017.04.013

Wang, Y. R., Zhang, B., Fan, J. L., Yang, Q., & Chen, H. Q. (2019). Effects of sodium tripolyphosphate modification on the structural, functional, and rheological properties of rice glutelin. *Food Chemistry, 281*, 18-27. https://doi.org/10.1016/j.foodchem.2018.12.085

Xiao, Y. Q., Li, J. M., Liu, Y. N., Peng, F., Wang, X. J., Wang, C., Li, M., & Xu, H. D. (2020). Gel properties and formation mechanism of soy protein isolate gels improved by wheat bran cellulose. *Food Chemistry, 324*, 1-8. https://doi.org/10.1016/j.foodchem.2020.126876

Xu, P., Qian, Y., Wang, R., Chen, Z., & Wang, T. (2022). Entrapping curcumin in the hydrophobic reservoir of rice proteins toward stable antioxidant nanoparticles. *Food Chemistry, 387*, 1-10. https://doi.org/10.1016/j.foodchem.2022.132906

Yang, S. F., Liu, L., Chen, H. Q., Wei, Y., Dai, L., Liu, J. F., Yuan, F., Mao, L., Li, Z. G., Chen, F., & Gao, Y. X. (2021). Impact of different crosslinking agents on functional properties of curcumin-loaded gliadin-chitosan composite nanoparticles. *Food Hydrocolloids, 112*, 1-11. https://doi.org/10.1016/j.foodhyd.2020.106258

Yao, Y. Y., Jia, Y. M., Lu, X. R., & Li, H. J. (2022). Release and conformational changes in allergenic proteins from wheat gluten induced by high hydrostatic pressure. *Food Chemistry, 368*, 1-11. https://doi.org/10.1016/j.foodchem.2021.130805

Zeng, Q. Z., Li, M. F., Li, Z. Z., Zhang, J. L., Wang, Q., Feng, S. L., Su, D. X., He, S., & Yuan, Y. (2019). Formation of gliadin-chitosan soluble complexes and coacervates through pH-induced: Relationship to encapsulation and controlled release properties. *Lwt-Food Science and Technology, 105*, 79-86. https://doi.org/10.1016/j.lwt.2019.01.071

Zhang, A. Q., He, J. L., Wang, Y., Zhang, X., Piao, Z. H., Xue, Y. T., & Zhang, Y. H. (2021). Whey protein isolate modified with sodium tripolyphosphate gel: A novel pH-sensitive system for controlled release of *Lactobacillus plantarum*. *Food Hydrocolloids, 120*, 1-8. https://doi.org/10.1016/j.foodhyd.2021.106924

Zhang, X., Wei, Z., Wang, X., Wang, Y., Tang, Q., Huang, Q., & Xue, C. (2022). Fabrication and characterization of core-shell gliadin/tremella polysaccharide nanoparticles for curcumin delivery: Encapsulation efficiency, physicochemical stability and bioaccessibility. *Current Research in Food Science, 5*, 288-297. https://doi.org/10.1016/j.crfs.2022.01.019

Zheng, W.-y., Wu, X.-m., Li, M.-x., Qiu, S.-l., Yang, T.-d., Yang, R., Chen, Z.-p., Wang, S.-y., & Liao, L. (2022). Synergistic strongly coupled super-deamidation of wheat gluten by glucose-organic acid natural deep eutectic solvent and the efficaciousness of structure and functionality. *Food Hydrocolloids, 125*, 1-13. https://doi.org/10.1016/j.foodhyd.2021.107437

Zhou, Y., Dhital, S., Zhao, C. Y., Ye, F. Y., Chen, J., & Zhao, G. H. (2021). Dietary fiber-gluten protein interaction

in wheat flour dough: Analysis, consequences and proposed mechanisms. *Food Hydrocolloids, 111*, 1-17. https://doi.org/10.1016/j.foodhyd.2020.106203

Zhu, X., Meng, L., Song, S., Ding, H., & Guo, Q. (2022). Insight into the mechanisms of the excellent emulsification properties of whey protein isolate-arabinoxylan conjugates. *Bioactive Carbohydrates and Dietary Fibre, 27*, 1-7. https://doi.org/10.1016/j.bcdf.2022.100312

Figure captions

Fig. 1. Effect of pH (A); WBC concentration (B); heating temperature (C), and adjusting time (D) on dispersibility index (PDI) and particle size (Dh) of WWBCs nanocomplexes. Dh and PDI (E), turbidity(F) changes of nanocomplexes with and without sodium tripolyphosphate (STP) modification. Error bars correspond to the standard deviation of triplicate studies. According to the least significant difference (LSD) multiple range, the alphabetic letters (a-d) indicated the mean values significantly different ($p < 0.05$).

Fig. 2. Characterization of wheat gluten proteins (WPs) bound to WBC: (A) endogenous fluorescence emission of WP and WWBCs at pH 7.0; (B) endogenous fluorescence emission of WWBCs 0.5 supplemented with 10 mm NaCl, SDS, and thiourea. Characterization of the molecular structures of WWBCs: (C) fluorescence emission of ANS bound to WWBCs 0.5 at pH 7-12; (D) fluorescence emission of ANS bound to WP and WWBCs; surface properties of WP, WBC and WWBCs; (E) hydrophobicity of WWBCs 0.5 at pH 7-12; (F) hydrophobicity of WP and WWBCs at pH 7; (G) Zeta-potential of WWBCs 0.5 at pH 7-12. (B) zeta-potential of WP, WBV and WWBCs at pH 7. Different letters close to bars indicate significant differences ($p < 0.05$).

Fig. 3. Detail of the morphology of WWBCs. (A-D) Transmission electron microscopy (TEM) micrographs of WP (A), WWBCs 0.1 (B), WWBCs 0.5 (C) and WWBCs 1.0 (D); The scale bar displayed in A1-D1 (bottom left corner) corresponds to 1μm. The micrographs of A2-D2 include a scale bar of 500 nm (a–d) AFM micrographs of WP (a), WWBCs 0.1 (b), WWBCs 0.5 (c) and WWBCs 1.0 (d).

Fig. 4. Scanning electron micrographs of WPs, WBC and WWBCs; (A) WBC; (B) WPs; (C) WWBCs 0.1; (D) WWBCs 0.5; (E) WWBCs 1.0, where 0.1, 0.5 and 0.5 correspond

to the mass ratio of WPs:WBC. The number 1 and 2 displayed in the label indicate that the images are magnified 500 and 20,000 times, respectively.

Fig. 5. UV spectra of curcumin at pH 12 at different reaction times. (A-D) UV spectra of curcumin; curcumin-WP mixture; curcumin-WBC mixture; and curcumin-WP-WBC mixture; respectively.

Fig. 6. Encapsulation efficiency (EE, %) (A) and encapsulation capacity (EC, mg/g) (B) of curcumin with different concentrations (0.2, 0.5, 1.0 and 2.0 mg/mL) by WWBCs prepared at different WPs:WBC ratios: 1:0.1,1:0.5, 1:1.0 (C). X-ray diffraction of curcumin before and after encapsulation. (D) FT-IR spectrum of curcumin, WPs, WBC, WWBCs with and without encapsulated curcumin. (E) Release profile of curcumin in WWBCs nanocomplexes under simulated gastrointestinal conditions. (F) DPPH radical scavenging activity of curcumin-loaded WWBCs nanocomplexes.

752 **Fig. 1**

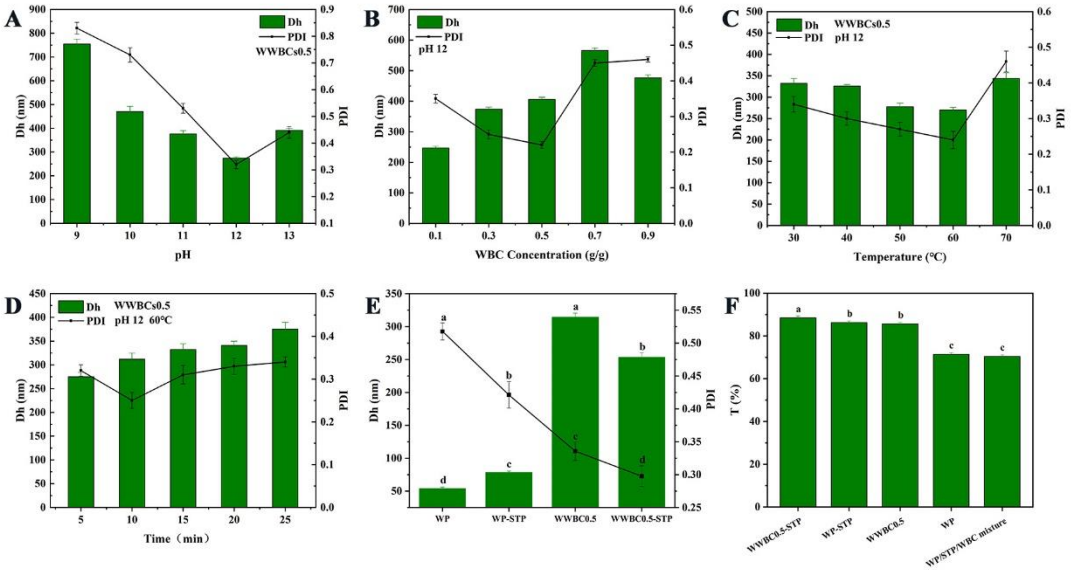

753

754

755 **Fig. 2**

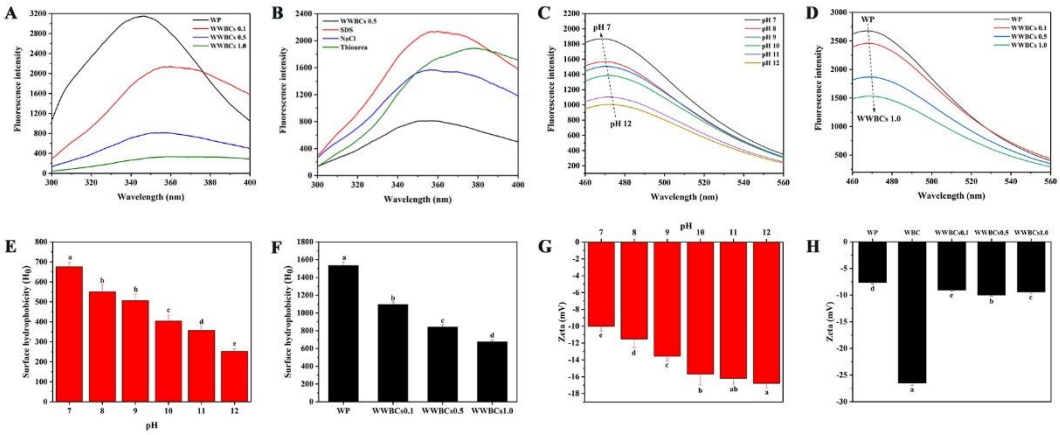

756

757

Fig. 3

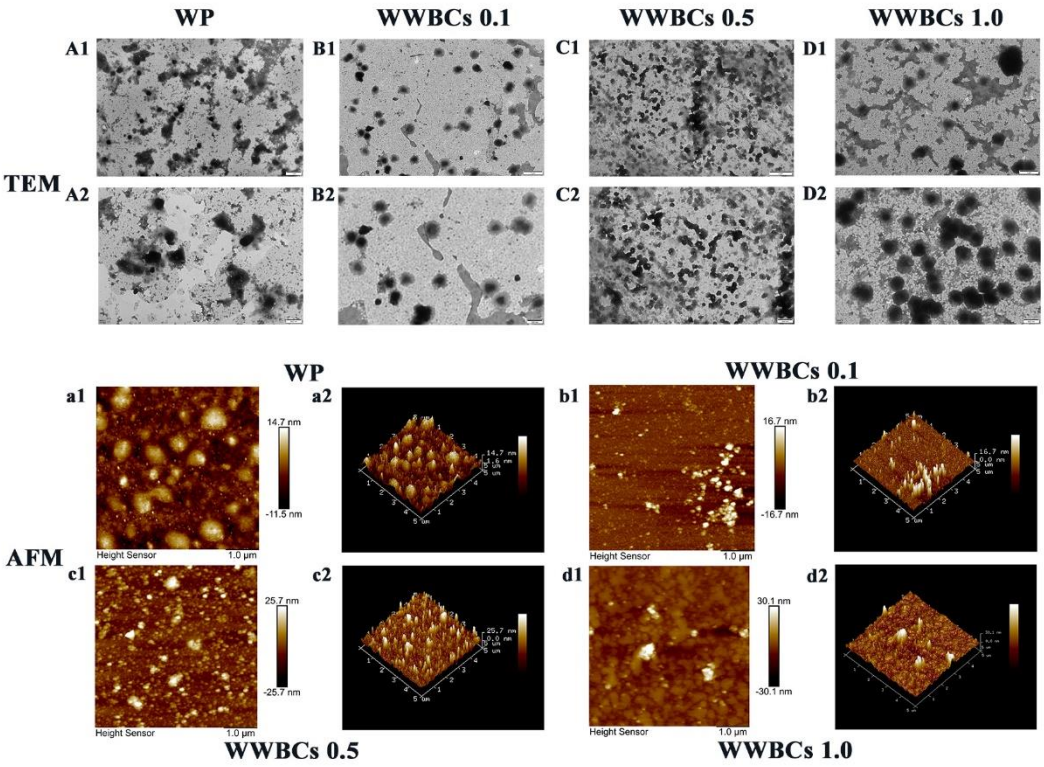
WP
WWBCs 0.1
WWBCs 0.5
WWBCs 1.0
TEM
A1
B1
C1
D1
A2
B2
C2
D2
AFM
a1
a2
b1
b2
c1
c2
d1
d2
14.7 nm
-11.5 nm
16.7 nm
-16.7 nm
25.7 nm
-25.7 nm
30.1 nm
-30.1 nm
Height Sensor
1.0 µm

761 **Fig. 4**

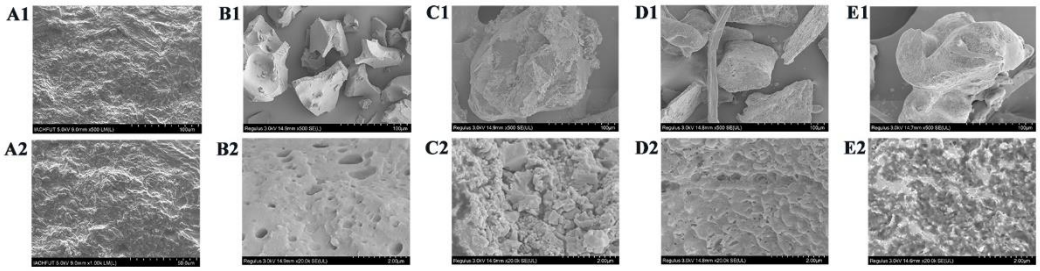

762

763

764 **Fig. 5**

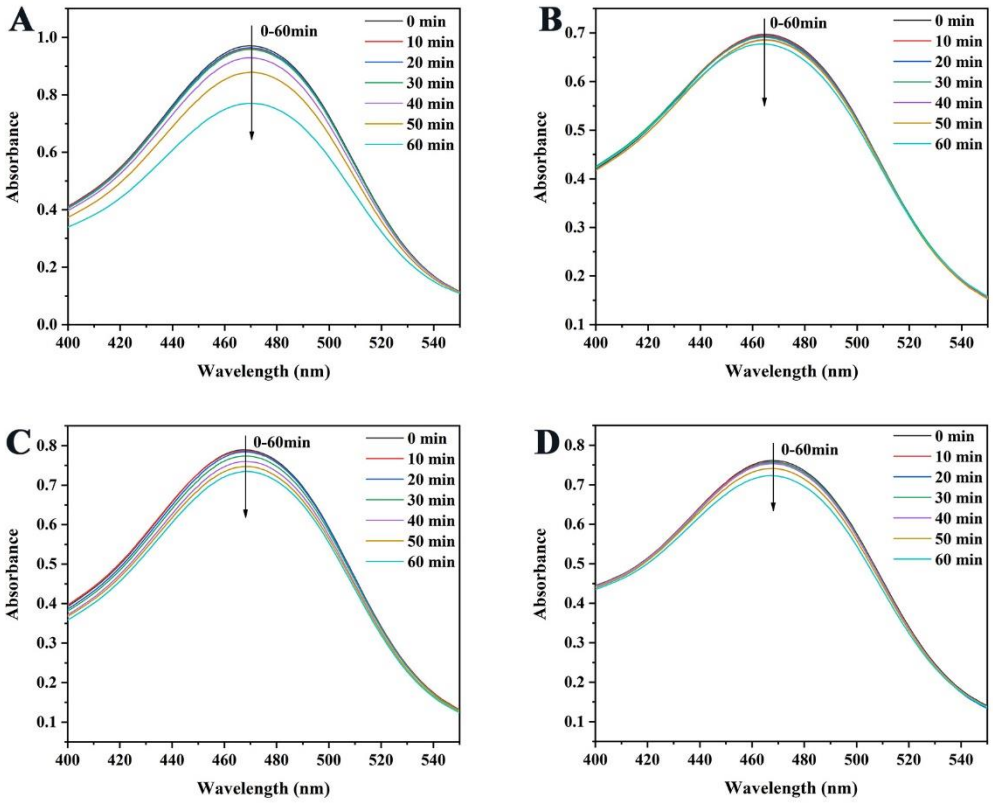

765

766

767 **Fig. 6**

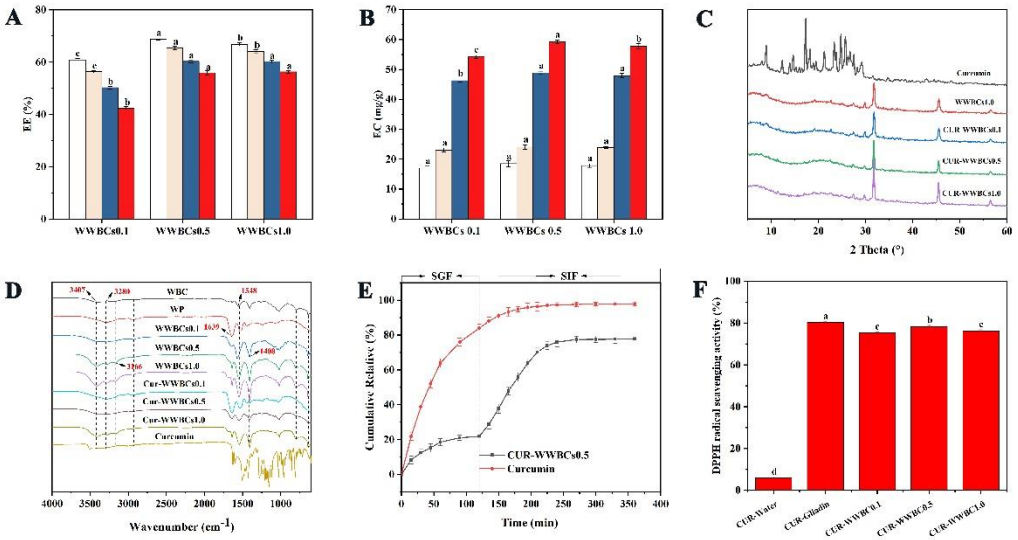

768

769

Supplemental Table 1. Thermal stability analysis of WWBCs composite with and without encapsulating curcumin.

Sample	Tp (℃)	ΔH (J/g)
WP	46.80±1.05f	17.39±1.11g
WWBCs0.1	50.46±1.28e	22.60±1.08f
WWBCs0.5	52.52±1.37de	27.27±1.56e
WWBCs1.0	53.57±1.32d	30.33±1.44d
Curcumin	179.49±2.11a	184.39±2.03a
Cur-WWBCs0.1	54.61±1.49cd	38.66±1.39c
Cur-WWBCs0.5	56.52±1.17bc	42.62±1.53b

Values in the same column followed by different letters (a–g) are significantly different ($P < 0.05$)